Behavior of $\chi^{(2)}$ during a laser-induced phase transition in GaAs

E. N. Glezer, Y. Siegal, L. Huang, and E. Mazur
Division of Applied Sciences and Department of Physics, Harvard University, Cambridge, Massachusetts 02138
(Received 6 September 1994)

We explicitly determine the second-order optical susceptibility of GaAs following intense femtosecond laser-pulse excitation from second-harmonic-generation measurements. To separate the dependence of the 4.4-eV second-harmonic signal on the second-order susceptibility from its dependence on the linear dielectric constant, we use experimentally determined values for the dielectric constant of GaAs at 2.2 and 4.4 eV. The results show that the excitation of electrons and the resulting changes in the lattice affect the behavior of the second-order susceptibility. At pump fluences of 0.6 kJ/m^2 and higher, the material loses long-range order on a time scale ranging from 100 femtoseconds to tens of picoseconds, depending on the pump fluence. A recovery of the second-order susceptibility to its initial value at pump fluences between 0.6 and 1.0 kJ/m^2 shows that the loss of long-range order is reversible in this fluence regime.

INTRODUCTION

Intense, femtosecond laser-pulse excitation of semiconductors provides a unique opportunity for observing the dynamics of a phase transition. The semiconductor-metal transition that can result from such excitation[1-11] is particularly interesting because it illustrates the critical role high free-carrier densities can play in modifying the electronic and structural properties of semiconductors. Understanding the complex dynamics involved in laser-induced phase transitions requires an explicit determination of the behavior of intrinsic material properties during these transitions.

Because of its sensitivity to crystal symmetry, second-harmonic generation has been used by a number of researchers to study laser-induced phase transitions in semiconductors.[3-7,12-14] The sensitivity of second-harmonic generation to the symmetry properties of a nonlinear crystal arises from the dependence of second-harmonic generation on the material's second-order optical susceptibility $\chi^{(2)}$, which reflects the symmetry group of the crystal.[15] A change in the material's symmetry properties, such as may occur in a phase transition, affects $\chi^{(2)}$ and results in a change in the detected second-harmonic signal. However, the detected second-harmonic signal depends on more material properties than just $\chi^{(2)}$. In particular, it depends also on the values of the linear optical susceptibility $\chi^{(1)}$ (or, equivalently, the linear dielectric constant ε) at both the fundamental frequency ω and the second-harmonic frequency 2ω of the probe beam used for second-harmonic generation.[15] Thus, to extract the behavior of $\chi^{(2)}$ from second-harmonic generation measurements, one must first know the behavior of $\varepsilon(\omega)$ and $\varepsilon(2\omega)$.

We combined experimental measurements of $\varepsilon(\omega)$ and $\varepsilon(2\omega)$ following intense femtosecond laser-pulse excitation of GaAs (Refs. 8–11) with second-harmonic generation measurements under identical excitation conditions to unambiguously determine the response of $\chi^{(2)}$ to this type of excitation. This experiment is unique because the response of $\chi^{(2)}$ to femtosecond laser-pulse excitation is extracted from second-harmonic-generation measurements by explicitly taking into account the experimentally determined response of $\chi^{(1)}$ to the same excitation rather than by assuming that the effect of $\chi^{(1)}$ on the second-harmonic-generation measurements is small. In fact, the experimentally-determined changes in $\chi^{(1)}$ are much larger than expected,[8-11] and our results show that these changes have a significant effect on the detected second-harmonic signal, contrary to earlier assumptions.[3,5,7] This effect masks the behavior of $\chi^{(2)}$ at fluences below 0.6 kJ/m^2, as will be discussed in Sec. III B. Expressly incorporating the changes in the dielectric constant in this experiment has uncovered previously unobserved behavior in this fluence range marked by recovery of $\chi^{(2)}$ to its initial value on a picosecond time scale.

I. $\chi^{(1)}$ AND $\chi^{(2)}$ DEPENDENCE OF SECOND-HARMONIC SIGNAL

While second-harmonic generation requires a nonzero $\chi^{(2)}$ in the dipole approximation, the dielectric constant ε also affects the strength of this process. The role of $\chi^{(2)}$ in second-harmonic generation is direct and straightforward: it determines the nonlinear polarization $P^{(2)}(2\omega)$, induced by an electric field $E(\omega)$, which acts as a source for the second-harmonic field $E(2\omega)$. The role of $\chi^{(1)}$ in second-harmonic generation is less direct but still very important. Changes in the dielectric constant can affect both $P^{(2)}(2\omega)$ itself as well as the amount of second-harmonic radiation produced by a given $P^{(2)}(2\omega)$.

The dielectric constant influences $P^{(2)}(2\omega)$ by affecting the orientation and magnitude of $E(\omega)$ relative to the crystallographic axes. As an example, if $E(\omega)$ is oriented in the y-z plane of a crystal and at an angle θ to the z axis, then the nonlinear polarization produced through $\chi^{(2)}_{xyz}$, the xyz element of the $\chi^{(2)}$ tensor, is given by

$$P^{(2)}_x(2\omega)=\chi^{(2)}_{xyz}E(\omega)\cos\theta E(\omega)\sin\theta=\chi^{(2)}_{xyz}E^2(\omega)\sin(2\theta)/2\ . \quad (1)$$

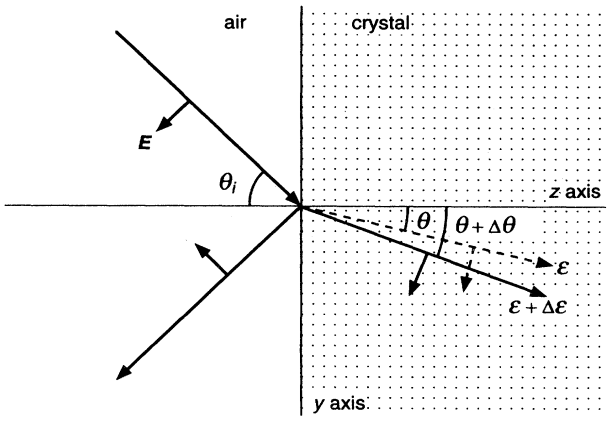

FIG. 1. Effect of a change in the dielectric constant of a material on the orientation of the electric field in the material relative to the crystallographic axes.

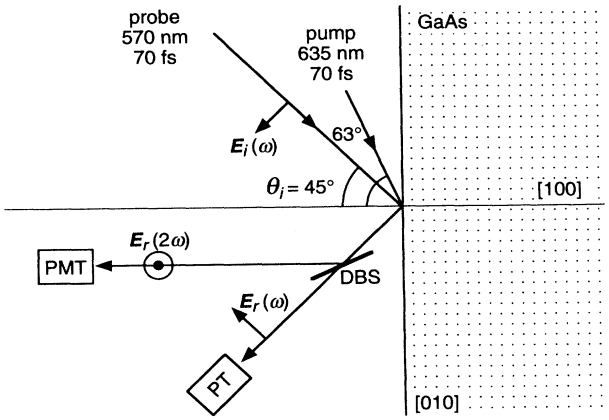

FIG. 2. Probing geometry for second-harmonic-generation measurements. A *p*-polarized probe beam in incident at 45° on a (100) GaAs sample in air. An ultraviolet mirror separates the reflected second-harmonic radiation, which is *s* polarized, from the reflected fundamental radiation, which is still *p* polarized. Notations are PMT (photomultiplier tube), PT (phototube), and DBS (dichroic beam splitter).

If the beam at frequency ω is initially incident on the crystal in the y-z plane at some fixed angle θ_i to the z axis, then, through Snell's Law, $\varepsilon(\omega)$ determines the angle θ inside the material that appears in Eq. (1), as shown in Fig. 1. Thus, changes in the dielectric constant affect $P^{(2)}(2\omega)$ through the dependence of $P^{(2)}(2\omega)$ on θ. In addition, through the Fresnel formulas for reflection and refraction, $\varepsilon(\omega)$ also determines the magnitude of the field in the material for a given incident field. Note that the field magnitude $E(\omega)$ appearing in Eq. (1) is the field magnitude inside the material, so changes in reflectivity can have a significant effect on $P^{(2)}(2\omega)$.

Besides its effect on the strength of $P^{(2)}(2\omega)$ itself, the dielectric constant also affects the amount of second-harmonic radiation generated from a given $P^{(2)}(2\omega)$ in a number of ways. First, the index of refraction, given by $n(\omega)=\mathrm{Re}[\varepsilon(\omega)^{1/2}]$, determines the phase velocity for light at frequency ω. The efficiency of second-harmonic generation depends on $n(\omega)-n(2\omega)$, which determines the phase mismatch between the induced nonlinear polarization and the resulting second-harmonic field: the larger the phase mismatch, the less efficient is second-harmonic generation.[15] The phase mismatch is important because it determines the length scale over which second-harmonic radiation generated by the propagating fundamental (frequency ω) beam adds with the proper phase to the propagating second-harmonic beam generated earlier along the beam path. Another way in which $\varepsilon(\omega)$ and $\varepsilon(2\omega)$ affect second-harmonic generation is by determining the absorption depth at ω and at 2ω. The absorption depth can affect second-harmonic generation by limiting the interaction length over which this process takes place.[15] If the energy depleted from the fundamental beam by second-harmonic generation is negligible, as it is in our experiment, then the total amount of second-harmonic generation produced is proportional to the square of the interaction length. So if the absorption depth at one or both of the frequencies becomes smaller than the interaction length, production of second-harmonic radiation will decrease accordingly. Finally, by modifying the reflection of the second-harmonic radiation at the surface of a material, changes in $\varepsilon(2\omega)$ affect the amount of second-harmonic radiation that gets out of the material.

Because GaAs absorbs in the visible and the ultraviolet, we carried out our second-harmonic-generation measurements in a reflection geometry, as illustrated in Fig. 2. One can derive an expression for the intensity of the reflected second-harmonic radiation as a function of $\varepsilon(\omega)$, $\varepsilon(2\omega)$, $\chi^{(2)}$, and the incident field magnitude $E_i(\omega)$ and angle θ_i of the fundamental beam. To do this, one must first solve the Maxwell equations for the electric-field amplitude inside the material, including the effects of the nonlinear polarization. Then, the amplitude of the reflected second-harmonic field is determined by imposing the proper boundary conditions at the surface and using a nonlinear generalization of Snell's Law.[15,16] For GaAs in the probing geometry illustrated by Fig. 2,[17] the reflected second-harmonic field amplitude is given by[15]

$$E_r(2\omega)=-4\pi P^{(2)}(2\omega)\left\{\frac{\sqrt{\varepsilon(\omega)-\sin^2\theta_i}-\sqrt{\varepsilon(2\omega)-\sin^2\theta_i}}{[\varepsilon(\omega)-\varepsilon(2\omega)][\sqrt{\varepsilon(2\omega)-\sin^2\theta_i}+\cos\theta_i]}\right\}, \tag{2}$$

where

$$P^{(2)}(2\omega)=2\chi^{(2)}E_i^2(\omega)\left\{\frac{4\sin\theta_i\cos^2\theta_i\sqrt{\varepsilon(\omega)-\sin^2\theta_i}}{\left[\varepsilon(\omega)\cos\theta_i+\sqrt{\varepsilon(\omega)-\sin^2\theta_i}\right]^2}\right\}. \tag{3}$$

The intensity of the reflected second-harmonic signal, and therefore the detected signal S, is proportional to $|E_r(2\omega)|^2$.

In the experiment presented here, we want to extract the behavior of $|\chi^{(2)}|^2$ following femtosecond laser-pulse excitation from measurements of the second-harmonic signal. In other words, we want to determine $|\chi^{(2)}(\phi,t)|^2$, where ϕ is the fluence of the excitation pulse and t is the time delay between the excitation pulse and the probe pulse. Note from Eqs. (2) and (3) that we can separate the dependence of the detected signal on the dielectric constant from its dependence on the second-order susceptibility as follows:

$$\frac{S}{|E_i^2(\omega)|^2}=F[\theta_i,\varepsilon(\omega),\varepsilon(2\omega)]|\chi^{(2)}|^2\ , \tag{4}$$

where the function $F[\theta_i,\varepsilon(\omega),\varepsilon(2\omega)]$ depends only on the dielectric constant and incident angle and not on the second-order susceptibility. We can define the normalized second-harmonic signal $S_{\rm norm}(\phi,t)\equiv S(\phi,t)/S(0,0)$, where $S(0,0)$ is the second-harmonic signal detected in the absence of any excitation. Similarly, we define $F_{\rm norm}(\phi,t)\equiv F(\phi,t)/F(0,0)$ and $\chi^{(2)}_{\rm norm}(\phi,t)\equiv\chi^{(2)}(\phi,t)/\chi^{(2)}(0,0)$. We can calculate $F_{\rm norm}(\phi,t)$ with values for $\varepsilon(\omega,\phi,t)$ and $\varepsilon(2\omega,\phi,t)$ determined experimentally using a two-angle reflectivity technique under similar laser-excitation conditions as in the measurements of $S_{\rm norm}(\phi,t)$ presented here.[8–11,18] Then, with the measured values of $S_{\rm norm}(\phi,t)$, we get from Eq. (4) values for $|\chi^{(2)}_{\rm norm}(\phi,t)|^2$:

$$|\chi^{(2)}_{\rm norm}(\phi,t)|^2=\frac{S_{\rm norm}(\phi,t)}{F_{\rm norm}(\phi,t)}\ . \tag{5}$$

Equation (5) allows us to extract the desired information on the behavior of the second-order susceptibility from our second-harmonic-generation measurements.

II. EXPERIMENTAL SETUP

The experiment presented in this paper consists of measurements carried out on an insulating (100) GaAs wafer (Cr-doped, $\rho>7\times10^7\ \Omega$ cm) in air. In this experiment, 70-fs, 1.9-eV (635-nm) pump pulses excite the sample and 70-fs, 2.2-eV (570-nm) probe pulses monitor second-harmonic generation and reflectivity at various time delays with respect to the excitation. To generate pump and probe pulses at different frequencies, we pass the amplified output of a colliding-pulse modelocked laser through a 20-mm, single-mode, polarization-preserving optical fiber.[19] Self-phase modulation in the fiber broadens the spectrum of the input pulse from 5 to 200 nm. By splitting this continuum beam with a broadband beam splitter, we can independently amplify different spectral regions within this 200-nm band width using two separate amplifier chains.[18] A three-stage amplifier using the dye DCM produces a 300-μJ pump beam centered at 635 nm with a 20-nm bandwidth; a two-stage amplifier using the dye Rhodamine 6G produces a 30-μJ probe beam centered at 570 nm with a 10-nm bandwidth. Both amplifiers are pumped by a frequency-doubled, 10-Hz Nd:YAG laser. Separate grating pairs compress each beam temporally to a final pulse width of 70 fs (full width at half maximum).

Figure 2 shows the probing geometry for the second-harmonic-generation measurements. The pump beam arrives at an incident angle of 63° with respect to the surface normal while the probe beam comes in with an incident angle of 45°. Both beams are polarized in the plane of incidence and are focused to the same spot on the sample. The (100) sample surface is set to a position with two of the crystallographic axes in the plane of incidence of the beams and the third one perpendicular to it. To monitor a uniformly excited region, we focus the probe beam more tightly than the pump beam: the probed surface area is about 25 times smaller than the 0.01-mm^2 focal area of the pump beam on the sample. Uniform excitation in the probed region is further assured by the small absorption depth of the second-harmonic radiation generated in the sample (about 20 nm) compared to that of the pump beam (270 nm). In the measurements of $\varepsilon(\omega)$ and $\varepsilon(2\omega)$ the absorption depth of the probe beams is also significantly shorter than the absorption depth of the pump beam.[11] The pump pulse fluence at each pump-probe time delay is varied over a range from 0 to 2.0 kJ/m^2. The probe beam fluence does not exceed 0.1 kJ/m^2 so as not to produce any detectable changes in the optical properties to within our experimental resolution. To avoid cumulative damage effects, we translate the sample during data collection so that each data point is obtained at a new spot on the sample.

To extract the behavior of the second-order susceptibility from the second-harmonic-generation measurements, we need to combine these measurements of $S_{\rm norm}(\phi,t)$ with the previous measurements of $\varepsilon(\omega,\phi,t)$ and $\varepsilon(2\omega,\phi,t)$, as described in Sec. I. We checked the consistency between the present data set and these previous measurements by simultaneously measuring the linear reflectivity along with the second-harmonic signal in the present experiment. To this end, we used a dichroic beam splitter to separate the second-harmonic radiation generated in reflection from the reflected fundamental radiation, measuring the second-harmonic signal using a photomultiplier tube and the fundamental signal with a calibrated phototube. The reflectivity values measured in this way agree with the reflectivity values we calculate for 45° incident angle and polarization in the plane of incidence using the measured dielectric constant from the previous set of data, verifying that the excitation conditions and fluence calibrations for both sets of measurements are indeed identical.

III. EXPERIMENTAL RESULTS

A. Effect of the linear optical susceptibility on the second-harmonic signal

Figure 3 summarizes the second-harmonic-generation measurements and highlights the importance of taking into account the effects of changes in the linear optical susceptibility on the second-harmonic signal. The filled circles in Fig. 3 represent the measured values of the normalized second-harmonic signal $S_{\text{norm}}(\phi,t)$ plotted versus pump fluence ϕ at four different pump-probe time delays t. The open circles in the figure represent the values of $F_{\text{norm}}(\phi,t)$ calculated using Eqs. (2)–(4) and the experimentally determined behavior of the dielectric constant at photon energies of 2.2 and 4.4 eV.[8–10,18] Note from Eq. (5) that the function $F_{\text{norm}}(\phi,t)$ is identical to $S_{\text{norm}}(\phi,t)$ if $\chi^{(2)}_{\text{norm}}(\phi,t)$ is held constant at its initial value of 1. In other words, $F_{\text{norm}}(\phi,t)$ (the open circles in Fig. 3) shows the changes that result in the second-harmonic signal *solely* from the behavior of $\chi^{(1)}$ following the excitation; it does not include any effects from changes in $\chi^{(2)}$.

As Fig. 3 shows, the changes induced in $\chi^{(1)}$ by the excitation have a significant impact on the measured second-harmonic signal, contrary to previous assumptions.[3,5,7] The locations of the minimum value of $F_{\text{norm}}(\phi,t)$ in each of the plots in Fig. 3 coincide with a large peak in the imaginary part of the dielectric constant at 2.2 eV described in previous papers.[8–11] The order of magnitude decrease in the absorption depth of the fundamental beam accompanying this peak in Im[ε(2.2 eV,ϕ,t)] plays a major role in the large drop in $F_{\text{norm}}(\phi,t)$ since its leads to a corresponding decrease in the interaction length for second-harmonic generation.[20] It is important to point out, however, that while the changes in $F_{\text{norm}}(\phi,t)$ play an important role in the behavior of $S_{\text{norm}}(\phi,t)$, $F_{\text{norm}}(\phi,t)$ never drops below the experimental noise and therefore cannot account for the vanishing of $S_{\text{norm}}(\phi,t)$. Thus, $\chi^{(2)}$ must go to zero for $S_{\text{norm}}(\phi,t)$ to reach zero.

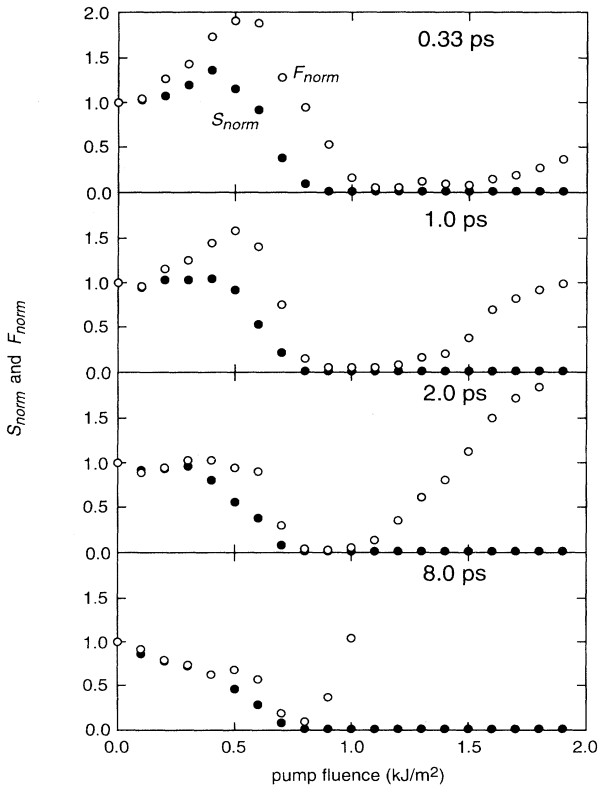

FIG. 3. Normalized second-harmonic signal vs pump fluence for four different pump-probe time delays. The data points are the measured second-harmonic signal, S_{norm} (●), and the second-harmonic signal calculated based solely on measured changes in dielectric constant, F_{norm} (○).

B. The response of $\chi^{(2)}$ to the excitation

According to Eq. (5), dividing $S_{\text{norm}}(\phi,t)$ (the filled circles in Fig. 3) by $F_{\text{norm}}(\phi,t)$ (the open circles in Fig. 3) yields $|\chi^{(2)}_{\text{norm}}(\phi,t)|^2$. The resulting values of $|\chi^{(2)}_{\text{norm}}(\phi)|^2$ appear in Fig. 4, shown at the same four pump-probe time delays as in Fig. 3. Figure 5 illustrates the time dependence of $|\chi^{(2)}_{\text{norm}}(t)|^2$ for various excitation strengths. The results exhibit a range of behaviors, depending on the excitation strength. At pump fluences of 0.8 kJ/m^2 and higher, $\chi^{(2)}$ goes to zero at a rate that increases with pump fluence: at 0.8 kJ/m^2 it takes about 2 ps to reach zero, while at 1.5 kJ/m^2 it reaches zero within a pump-

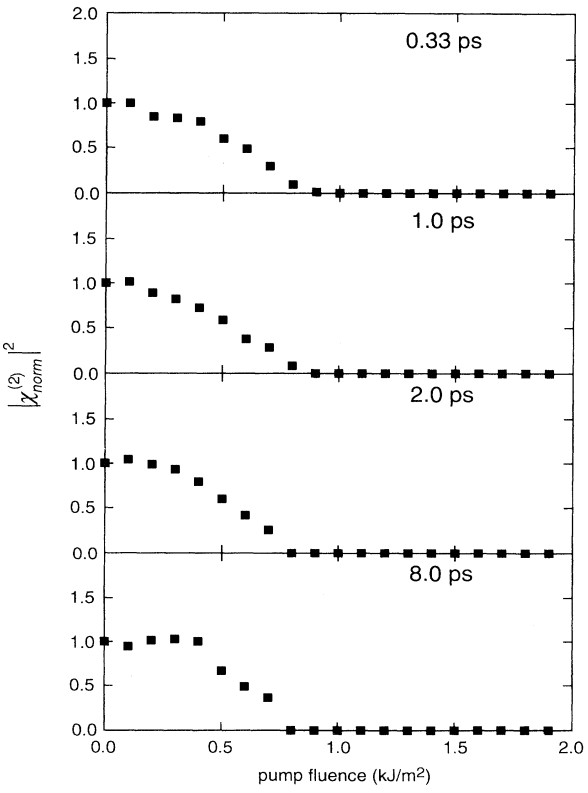

FIG. 4. Square of the second-order susceptibility vs pump fluence for four different pump-probe time delays.

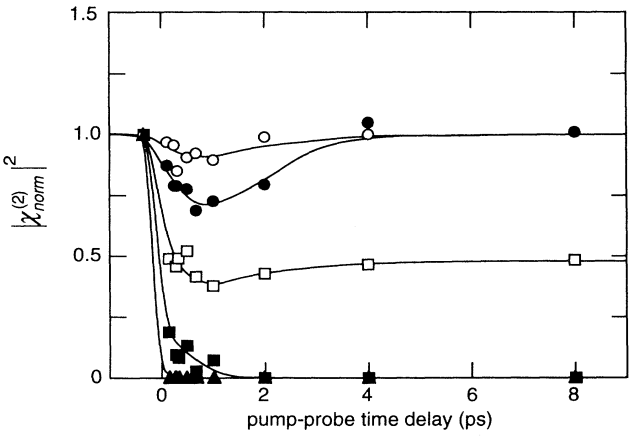

FIG. 5. Square of the second-order susceptibility vs pump-probe time delay for various pump fluences. The curves are drawn to guide the eye. ○: 0.2 kJ/m^2; ●: 0.4 kJ/m^2; □: 0.6 kJ/m^2; ■: 0.8 kJ/m^2; ▲: 1.5 kJ/m^2.

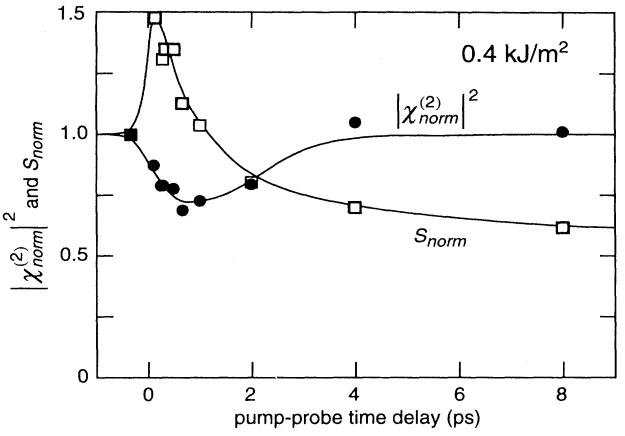

FIG. 6. Normalized second-harmonic signal (□) and square of the second-order susceptibility (●) vs pump-probe time delay at a pump fluence of 0.4 kJ/m^2. The curves are drawn to guide the eye.

probe time delay of 130 fs. In contrast, at pump fluences less than or equal to 0.6 kJ/m^2 , $\chi^{(2)}$ undergoes a partial decrease, but it does not reach zero. For pump fluences below 0.5 kJ/m^2, $\chi^{(2)}$ recovers to its initial value on a time scale of a few picoseconds.

Since $\chi^{(2)}$ must go to zero for $S_{\rm norm}(\phi,t)$ to reach zero, the behavior of $S_{\rm norm}$ at fluences for which it drops to zero is similar to that of $\chi^{(2)}$. Thus, for high fluences the conclusions from previous second-harmonic-generation experiments, in which changes in the dielectric constant are not explicitly taken into account, agree at least qualitatively with our $\chi^{(2)}$ data.[3–7] In contrast, the behavior we observe at lower fluences has not been reported before. At fluences for which $\chi^{(2)}$ does not reach zero, it is particularly important to account for the effects of changes in the dielectric constant on the measured second-harmonic signal. In fact, Fig. 6 shows that the $S_{\rm norm}$ measurements at a fluence of 0.4 kJ/m^2 are actually misleading if one assumes that the behavior of $|\chi^{(2)}_{\rm norm}|^2$ is given directly by the second-harmonic signal. Under this assumption, one would conclude from Fig. 6 that at this fluence $|\chi^{(2)}_{\rm norm}|^2$ first rises and then drops below its initial value within a few picoseconds. However, our results show that at these fluences $|\chi^{(2)}_{\rm norm}|^2$ first *decreases* and then *recovers* to its initial value within a few picoseconds.

C. Long-time behavior: Reversible versus irreversible changes

Although we focused our attention on the behavior of $\chi^{(2)}$ during the first 10 ps following the excitation, we also measured both the second-harmonic signal and the linear reflectivity at a time delay of a few seconds, after the material has reached its final state, shown in Fig. 7(a), as well as the second-harmonic signal at a pump-probe time delay of 100 ps, shown in Fig. 7(b). Figure 7(a) shows a sharp demarcation at 1.0 kJ/m^2 in the final state of $\chi^{(2)}$. For excitation strengths below 1.0 kJ/m^2, both the second-harmonic signal and the linear reflectivity eventually return to their initial values.[21] However, neither the

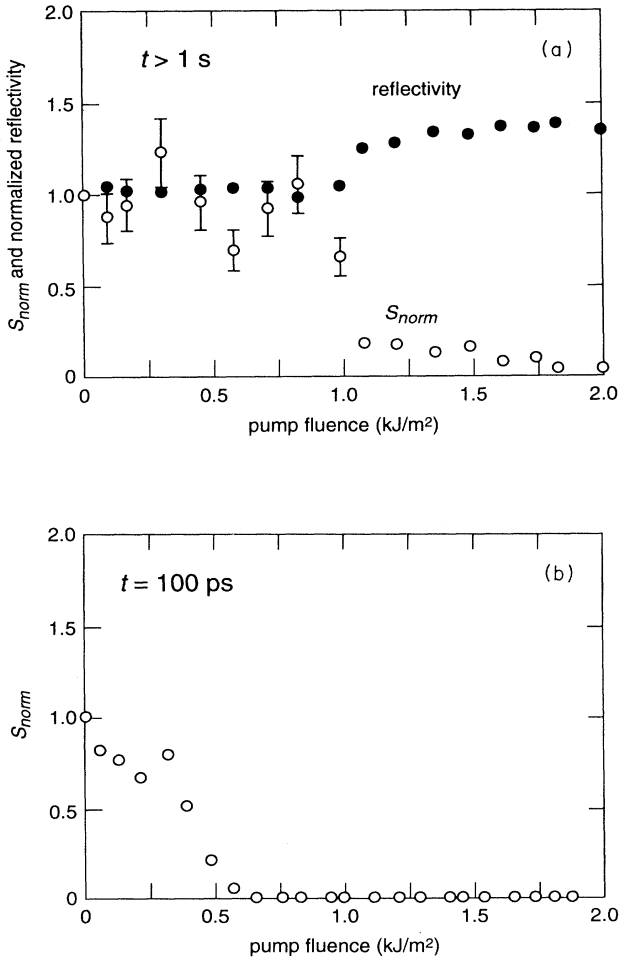

FIG. 7. (a) Normalized second-harmonic signal (○) and normalized 45° reflectivity (●) at a time delay of a few seconds, after the material has reached its final state. (b) Normalized second-harmonic signal vs pump fluence at time delay of 100 ps.

second-harmonic signal nor the linear reflectivity ever returns to its initial value for pump fluences above 1.0 kJ/m^2. Thus, the changes induced in the material by the laser-pulse excitation are reversible if the pump fluence is below 1.0 kJ/m^2 but are irreversible if the pump fluence is above 1.0 kJ/m^2. This conclusion is consistent with an examination of the sample through a microscope. By correlating pump pulse fluence with the size of damage spots on the sample measured through the microscope, we determined a threshold fluence for permanent damage of 1.0 kJ/m^2, in agreement with the threshold for irreversible change evident in Fig. 7(a). Figure 7(b) shows that for fluences greater than 0.6 kJ/m^2, once S_{norm} vanishes, it remains zero for at least 100 ps. Thus, the recovery of $\chi^{(2)}$ to its initial value at fluences between 0.6 and 1.0 kJ/m^2 occurs on a time scale which is orders of magnitude larger than the recovery times for fluences less than or equal to 0.5 kJ/m^2.

IV. DISCUSSION

A. Three regimes of behavior

The results presented in the preceding section suggest three main regimes of behavior for $\chi^{(2)}$ following laser-pulse excitation. In the low-fluence regime, below 0.5 kJ/m^2, $\chi^{(2)}$ exhibits a partial drop but recovers to its initial value within a few picoseconds. At medium fluences, from roughly 0.8 to 1.0 kJ/m^2, $\chi^{(2)}$ drops to zero on a time scale between a few hundred femtoseconds and a few picoseconds and remains zero for over 100 ps, but eventually also recovers to its initial value. In the high-fluence regime, above 1.0 kJ/m^2, $\chi^{(2)}$ drops to zero within a few hundred femtoseconds and never recovers to its initial value. While a clear boundary at 1.0 kJ/m^2 separates the medium- and higher-fluence regimes, no clear boundary separates the low- and medium-fluence regimes. Rather, the behavior gradually changes from low-fluence behavior to medium-fluence behavior between 0.5 and 0.8 kJ/m^2.

The recovery time scale in the low-fluence range suggests that the behavior of $\chi^{(2)}$ in this range is likely dominated by electronic effects. The laser-pulse excitation of electrons from the valence to the conduction band can directly affect $\chi^{(2)}$ in a number of ways. First, delocalized conduction electrons contribute little to $\chi^{(2)}$ in GaAs compared to localized valence electrons.[22–24] Thus, we expect the excitation of a high density of electrons from the valence band to the conduction band by the pump pulse ($>10^{21}$ cm^{-3}) to cause a drop in $\chi^{(2)}$. Second, the excited free carriers can also reduce the valence-band contribution to $\chi^{(2)}$ by bleaching resonant transitions, due to phase-space filling. In addition, electronic screening of the ionic potential by the free carriers will modify the electronic band structure,[25] further affecting the valence-band contribution to $\chi^{(2)}$. Because the magnitude of these electronic effects should depend on the free-carrier density, we expect $\chi^{(2)}$ to return to its initial value as the excited free-carrier density relaxes through Auger recombination and diffusion following the excitation. The picosecond time scale for the observed recovery of $\chi^{(2)}$ in the low-fluence regime agrees with the time scale for Auger recombination and diffusion at free-carrier densities on the order of 10^{21} cm^{-3}.[26,27] While the low-fluence recovery time is consistent with the expected behavior of the free-carrier population, the source of the initial 1-ps delay between the excitation and the maximum change in $\chi^{(2)}$ in this fluence regime is unclear. One possible cause for this delay is that in addition to its dependence on the free-carrier density, $\chi^{(2)}$ may be strongly affected by the distribution of the free carriers in the energy bands. In this case, continued heating of the free-carrier population by Auger recombination may counteract the effects of carrier density relaxation in the picosecond following the excitation and result in the observed behavior. Alternatively, it is possible that in this fluence regime the electronic excitation drives a slight structural distortion in the lattice, which is reversed when the carrier density decreases through recombination. If it is a temporary distortion of the lattice that is responsible for the partial drop in $\chi^{(2)}$, the picosecond delay in the drop would result from the time scale of the atomic motion.

Structural changes in the lattice most likely dominate the behavior of $\chi^{(2)}$ in the medium- and high-fluence regimes. The time dependence of $\chi^{(2)}$ in these two regimes is not consistent with electronic time scales. First of all, the recovery time for $\chi^{(2)}$ is greater than 100 ps in the medium-fluence regime compared with electronic relaxation times of a few picoseconds in the low-fluence regime. Moreover, the drop in $\chi^{(2)}$ to zero at fluences greater than 0.6 kJ/m^2 cannot be accounted for by the roughly 10% valence band depopulation achieved by the pump pulse.[24] A structural change in the lattice, however, could lead to a vanishing of $\chi^{(2)}$ on the observed time scales.[28] Recovery times for reversible structural changes should be comparable to lattice relaxation times, which are much greater than 100 ps.[29]

B. Loss of long-range order

What does the vanishing of $\chi^{(2)}$ imply about the structural changes in the lattice induced by the pump pulse? In the dipole approximation, $\chi^{(2)}=0$ in materials that have a center of inversion.[15] However, the loss of bulk, dipole $\chi^{(2)}$ does not necessarily mean that the material has taken on a true center of inversion within each unit cell. A loss of long-range order on the scale of the wavelength of light is sufficient to cause such a drop in $\chi^{(2)}$. Experiments show that the degree of amorphization induced by low-dosage ion implantation (1×10^{12}–6×10^{15} cm^{-2} integrated flux of 80-keV Te^+ and S^+ ions) leads to a one-to-two order-of-magnitude drop in $\chi^{(2)}$.[24] The extent of ionic motion required for GaAs to lose long-range order is much smaller than that required for GaAs to take on a local center of inversion in each unit cell. Given the time scales involved in the data, a loss of long-range order is the most likely explanation for the observed drop in $\chi^{(2)}$ to zero in the medium- and high-fluence regimes.

The data in Figs. 4, 5, and 7(b) then support the conclusion that, for pump fluences greater than 0.6 kJ/m^2,

the pump pulse induces an instability in the covalent bonding of GaAs that leads to structural change in the lattice. The instability, which results from the excitation of a critical density of electrons from bonding valence states to antibonding conduction states,[28,30,31] occurs instantaneously with the generation of free carriers. Because the zinc-blende structure is no longer stable, the ions start to move away from their ground-state positions. As the ions start to move, the material loses its long-range order, and $\chi^{(2)}$ goes to zero. A stronger excitation results in a greater instability and, therefore, faster ionic motion and a faster drop in $\chi^{(2)}$. This interpretation of the data is consistent with the previous set of dielectric constant measurements mentioned in Sec. I. The dielectric constant data, which indicate a collapse of the band gap caused by structural changes in the lattice, are fully discussed in other papers.[8–11]

In light of the above interpretation, the material exhibits a particularly interesting response to the excitation in the medium-fluence regime. As discussed in Sec. III C, pump fluences greater than the damage threshold of 1.0 kJ/m^2 induce irreversible changes in the material, while the changes for pump fluences below this threshold are reversible. Thus, in the medium-fluence range the crystal *reversibly* undergoes sufficiently large structural changes to lose its long-range order. The ability to induce such large *transient* changes in a semiconductor's structural, electronic, and optical properties may be relevant for the development of optoelectronic switching devices.

V. CONCLUSION

We determined the behavior of $\chi^{(2)}$ following femtosecond laser-pulse excitation from second-harmonic generation measurements by explicitly taking into account the effect of changes in the linear dielectric constant on the second-harmonic signal. We find that accounting for the changes in the linear dielectric constant is particularly important for pump fluences at which $\chi^{(2)}$ does not vanish, because the changes in the second-harmonic signal at these fluences do not mirror the changes in $\chi^{(2)}$. The results show three regimes of behavior: (1) at low fluences, below 0.5 kJ/m^2, $\chi^{(2)}$ exhibits a partial drop and a recovery to its initial value within a few picoseconds; (2) at medium fluences, between 0.8 and 1.0 kJ/m^2, $\chi^{(2)}$ drops to zero but recovers to its initial value on a time scale greater than 100 ps; and (3) at high fluences, above 1.0 kJ/m^2, $\chi^{(2)}$ vanishes and never recovers to its initial value.

The structural changes that follow the laser-pulse excitation in the medium- and high-fluence regimes result from the destabilization of the covalent bonds by the excitation. The resulting ionic motion leads to a loss of long-range order, as indicted by the vanishing of $\chi^{(2)}$. This loss of long-range order is observed even at pump fluences below the damage threshold of 1.0 kJ/m^2, a regime in which the induced changes are reversible.

ACKNOWLEDGMENTS

We appreciate many useful discussions with Professor N. Bloembergen, Professor H. Ehrenreich, and Professor M. Aziz. E.N.G. gratefully acknowledges financial support from the Fannie and John Hertz Foundation. This work was supported by Contracts Nos. ONR N00014-89-J-1023 and NSF DMR 89-20490.

[1]C. V. Shank, R. Yen, and C. Hirlimann, Phys. Rev. Lett. **50**, 454 (1983).

[2]M. C. Downer, R. L. Fork, and C. V. Shank, J. Opt. Soc. Am. B **2**, 595 (1985).

[3]H. W. K. Tom, G. D. Aumiller, and C. H. Brito-Cruz, Phys. Rev. Lett. **60**, 1438 (1988).

[4]T. Schröder, W. Rudolph, S. V. Govorkov, and I. L. Shumai, Appl. Phys. A **51**, 1438 (1990).

[5]S. V. Govorkov, I. L. Shumay, W. Rudolph, and T. Schroeder, Opt. Lett. **16**, 1013 (1991).

[6]K. Sokolowski-Tinten, H. Schulz, J. Bialkowski, and D. von der Linde, Appl. Phys. A **53**, 227 (1991).

[7]P. N. Saeta, J. Wang, Y. Siegal, N. Bloembergen, and E. Mazur, Phys. Rev. Lett. **67**, 1023 (1991).

[8]Y. Siegal, E. N. Glezer, and E. Mazur, Phys. Rev. B **49**, 16 403 (1994).

[9]Y. Siegal, E. N. Glezer, I. Huang, and E. Mazur, in *Ultrafast Phenomena in Semiconductors,* edited by D. K. Ferry and H. M. van Driel (SPIE, Bellingham, Washington, 1994).

[10]Y. Siegal, E. N. Glezer, and E. Mazur, in *Femtosecond Chemistry,* edited by J. Manz and L. Wöste (Verlag Chemie, Berlin, 1994).

[11]E. N. Glezer, Y. Siegal, L. Huang, and E. Mazur, Phys. Rev. B **51**, 6959 (1995).

[12]C. V. Shank, R. Yen, and C. Hirlimann, Phys. Rev. Lett. **51**, 900 (1983).

[13]J. M. Liu, A. M. Malvezzi, and N. Bloembergen, in *Energy Beam-Solid Interactions and Transient Thermal Processing,* edited by D. K. Biegelsen, G. A. Rozgonyi, and C. V. Shank (Materials Research Society, Pittsburgh, 1985).

[14]S. A. Akhmanov, V. I. Emel'yanov, N. I. Koroteev, and V. N. Seminogov, Usp. Fiz. Nauk **147**, 675 (1985) [Sov. Phys. Usp. **28**, 1084 (1985)].

[15]Y. R. Shen, *Principles of Nonlinear Optics* (Wiley, New York, 1984).

[16]N. Bloembergen and P. S. Pershan, Phys. Rev. **128**, 606 (1962).

[17]In this case, $\chi^{(2)}_{xyz}$ is the only element of the $\chi^{(2)}$ tensor that contributes to the second-harmonic generation.

[18]Y. Siegal, Ph.D. thesis, Harvard University, 1994.

[19]J. K. Wang, Y. Siegal, C. Z. Lü, and E. Mazur, Opt. Commun. **91**, 77 (1992).

[20]While a drop in the penetration depth certainly reduces the bulk dipole contribution to the second-harmonic generation, its effect on the bulk quadrupole contribution is more complicated. The complication arises from the dependence of the quadrupole contribution to second-harmonic generation on the electric-field gradient, which increases as the penetration depth decreases. More generally, Eq. (3), which gives the dependence of the nonlinear polarization on the dielectric constant, applies only to bulk dipole second-harmonic generation. An appropriate expression must be substituted for Eq. (3) to analyze second-harmonic-generation experiments on

centrosymmetric materials such as Si, where quadrupole contributions are important (such as in Ref. 3).

[21]The noise apparent in the S_{norm} data at a pump-probe time delay of a few seconds [see Fig. 7(a)] stems from the photomultiplier tube we used to detect the second-harmonic signal. At other time delays, we collected enough data to improve the signal-to-noise ratio through averaging—the noise in the other S_{norm} data [see Figs. 3 and 7(b)] is comparable to the size of the data point symbol. However, we have fewer data points at the final-state time delay, limiting the reduction in noise achievable through averaging.

[22]N. Bloembergen, R. K. Chang, S. S. Jha, and C. H. Lee, Phys. Rev. **174**, 813 (1968).

[23]S. A. Akhmanov, N. I. Koroteev, G. A. Paitan, I. L. Shumay, M. V. Galjautdinov, I. B. Khaibulllin, and E. I. Shtyrkov, Opt. Commun. **47**, 202 (1983).

[24]S. A. Akhmanov, M. F. Galyautdinov, N. I. Koroteev, G. A. Paityan, I. B. Khaibullin, E. I. Shtyrkov, and I. L. Shumai, Izv. Akad. Nauk. SSSR Ser. Fiz. **49**, 506 (1985) [Bull. Acad. Sci. USSR, Phys. Ser. **49**, 86 (1985)].

[25]D. H. Kim, H. Ehrenreich, and E. Runge, Solid State Commun. **89**, 119 (1994).

[26]E. J. Yoffa, Phys. Rev. B **21**, 2415 (1980).

[27]H. M. van Driel, Phys. Rev. B **35**, 8166 (1987).

[28]P. Stampfli and K. H. Bennemann, Phys. Rev. B **42**, 7163 (1990).

[29]F. Spaepen, in *Ultrafast Phenomena V,* edited by G. R. Fleming and A. E. Siegman (Springer-Verlag, Berlin, 1986).

[30]J. A. Van Vechten, R. Tsu, and F. W. Saris, Phys. Lett. **74A**, 422 (1979).

[31]R. Biswas and V. Ambegoakar, Phys. Rev. B **26**, 1980 (1982).